J Biomol NMR (2009) 45:373–387
DOI 10.1007/s10858-009-9380-5

ARTICLE

Analysis of the amide ^{15}N chemical shift tensor of the C_α tetrasubstituted constituent of membrane-active peptaibols, the α-aminoisobutyric acid residue, compared to those of di- and tri-substituted proteinogenic amino acid residues

Evgeniy Salnikov · Philippe Bertani · Jan Raap · Burkhard Bechinger

Received: 20 May 2009 / Accepted: 11 September 2009 / Published online: 11 October 2009

Abstract In protein NMR spectroscopy the chemical shift provides important information for the assignment of residues and a first structural evaluation of dihedral angles. Furthermore, angular restraints are obtained from oriented samples by solution and solid-state NMR spectroscopic approaches. Whereas the anisotropy of chemical shifts, quadrupolar couplings and dipolar interactions have been used to determine the structure, dynamics and topology of oriented membrane polypeptides using solid-state NMR spectroscopy similar concepts have been introduced to solution NMR through the measurements of residual dipolar couplings. The analysis of ^{15}N chemical shift spectra depends on the accuracy of the chemical shift tensors. When investigating alamethicin and other peptaibols, i.e. polypeptides rich in α-aminoisobutyric acid (Aib), the ^{15}N chemical shift tensor of this C_α-tetrasubstituted amino acid exhibits pronounced differences when compared to glycine, alanine and other proteinogenic residues. Here we present an experimental investigation on the ^{15}N amide Aib tensor of *N*-acetyl-Aib-OH and for the Aib residues within peptaibols. Furthermore, a statistical analysis of the tensors published for di- (glycine) and tri-substituted residues has been performed, where for the first time the published data sets are compiled using a common reference. The size of the isotropic chemical shift and main tensor elements follows the order di- < tri- < tetra-substituted amino acids. A ^{15}N chemical shift-^{1}H-^{15}N dipolar coupling correlation NMR spectrum of alamethicin is used to evaluate the consequences of variations in the main tensor elements for the structural analysis of this membrane peptide.

Keywords Oriented membranes · Oriented bicelles · Chemical shift anisotropy · Oriented lipid bilayer · α-Helix · 3_{10} Helix · Membrane protein structure determination · Topology · Angular restraints · Tilt and rotational pitch angle

E. Salnikov · P. Bertani · B. Bechinger (✉)
Institut de Chimie, Université de Strasbourg/CNRS, UMR7177, 4, rue Blaise Pascal, 67070 Strasbourg, France
e-mail: bechinge@unistra.fr

J. Raap
Leiden Institute of Chemistry, Gorlaeus Laboratories, Leiden University, Einsteinweg 55, P.O. Box 9502, 2300 RA Leiden, The Netherlands

Introduction

The chemical shift interaction is an important parameter that provides information on the functional groups and the detailed chemical environment in many molecules including proteins. Because of spatial variation in electron density the chemical shift interactions are inherently anisotropic. For small and medium sized proteins in isotropic solutions this orientation-dependence is averaged by rotational diffusion. However, in solids or in soft solids, averaging is absent, incomplete or directional and, therefore, the chemical shift is a function of the alignment of the molecules relative to the magnetic field direction (Mehring 1983). Notably, this orientation dependence is quite pronounced as, for example, the anisotropy of the ^{15}N resonance of an amide within a peptide bond is an order of magnitude increased when compared to the isotropic chemical shift dispersion typically observed for protein amides in aqueous solution [a comparison is shown in Fig. 2 of (Bechinger and Sizun 2003)].

The chemical shift anisotropy thereby provides a valuable parameter for the analysis of the structure of proteins and allows the investigation of their local and globular

dynamics (Aisenbrey and Bechinger 2004; Bechinger 2009; Cady et al. 2007; Dürr et al. 2007). In particular in samples that have been uniaxially aligned relative to the magnetic field direction such as liquid crystals or lipid bilayers the chemical shift anisotropy has been exploited for the structural analysis of polypeptides in macromolecular complexes such as biological membranes using solid-state NMR spectroscopy [e.g. (Bechinger et al. 1993; Cross 1997; Aisenbrey et al. 2006; Opella et al. 2008)]. Furthermore, weakly orienting media have been introduced to solution NMR spectroscopy that allow for the observation of residual dipolar couplings of a few Herz and small chemical shift alterations when at the same time fast averaging ensures the narrow line shapes that result in high resolution NMR spectra [reviewed in (Lipsitz and Tjandra 2004; Prestegard et al. 2004; Bax and Grishaev 2005; Tolman and Ruan 2006; Prosser et al. 2006)].

The analysis of data from strongly or weakly oriented samples depends on a good understanding of the size and spatial properties of the underlying interaction anisotropies. The chemical shift interaction is mathematically described by second rank tensors and the knowledge of the size of their main components and their alignment within the molecular frame are important for the calculation of orientational restraints. Furthermore, the trace of the tensor provides the isotropic value of the chemical shift interaction. Therefore many data have been published on the ^{15}N chemical shift tensors of amide bonds within small peptides or within model compounds, with focus on the peptide bonds involving the nitrogens of glycine, L-alanine or other 'conventional' amino acids (Table 1, cf. Discussion section of this paper for a more detailed analysis). The orientation of the amide ^{15}N chemical shift tensor in the peptide molecular frame is shown in Fig. 1.

When peptides containing α-aminoisobutyric acids were investigated by solution or solid-state NMR spectroscopy it was soon realized that this amino acid exhibits different isotropic and anisotropic chemical shift properties when compared to 'conventional' amino acids (Salnikov et al. 2009; Yee and O'Neil 1992). There is considerable interest in membrane polypeptides containing the Aib residues as these peptaibols have been among the first polypeptides that could be analysed by a variety of membrane biophysical methods [reviewed in (Sansom 1993; Bechinger 1997)]. The study of one of them, namely alamethicin, has early on suggested that the association of several polypeptides in the form of transmembrane helical bundles can explain the single-channel properties observed in the presence of this peptide or of large membrane proteins (Sansom 1993; Bechinger 1997). Furthermore, the investigation of alamethicin has shaped our view on polypeptide-membrane interactions, as well as on the antimicrobial and channel-forming properties of related compounds. Although proton-decoupled ^{15}N solid-state NMR spectroscopy of oriented membrane samples has already provided valuable insights about the conformation and topology of membrane-associated peptaibols [e.g. (Salnikov et al. 2009; North et al. 1995; Vosegaard et al. 2008)] many details of their structure and dynamics in phospholipids bilayers remain to be clarified. In order to analyse such one- and two-dimensional solid-state NMR data obtained from labelled peptaibols, a better description of the Aib tensor, an amino acid that is highly abundant in these peptides (ca. 40%), is required. Therefore, we performed a number of experiments on model compounds and peptides that allowed us to better characterize the ^{15}N chemical shift tensor of peptide bonds involving Aib. In parallel, an extensive analysis of the published tensors of glycine and other conventional amino acids is presented where special emphasis has been made to standardize the different calibrations of the ^{15}N chemical shifts published by the different laboratories over the years (Table 1).

Materials and methods

Preparation of ^{15}N-amino acid derivatives. To synthesize ^{15}N-acetyl-α-aminoisobutyric acid ([^{15}N]-Ac-Aib-OH) a solution of 1 g of [^{15}N]-Aib (99% ^{15}N) (Ogrel et al. 2000) in 50 ml of 3 M HCl/*n*-butanol was boiled for 5 h. After cooling down the reaction mixture was filtrated over a glass filter and the solvent was evaporated in vacuo. To the oily residue 30 ml of acetic acid and 3.0 ml of acetic acid anhydride was added followed by heating under reflux during 3 h. The solvents were removed by evaporation using an oil pump and the last traces of acid were removed by azeotropic distillation of a toluene solution of the residue. The [^{15}N]-Ac-Aib-*n*-butyl ester was treated with aqueous NaOH until pH = 12 followed by stirring the reaction mixture overnight at room temperature. After cooling with ice and acidification with 6 M HCl the product was isolated by extraction with *n*-butanol and evaporation of the solvent. The solid compound was taken up in ethyl acetate and the solution was dried on $MgSO_4$. Crystal needles were obtained after addition of diethylether and petroleum ether.

^{1}H-NMR (600 MHz, $CDCl_3/CD_3OD$, internal chemical shift standard tetramethylsilane, δ in ppm): δ 1.31 (s, 6H, $(CH_3)_2$), δ 1.85 (s, 3H, $AcCH_3$), δ 7.54 (d, 1H, $^1J_{NH}$ 90.3 Hz, ^{15}N-H); ^{13}C-NMR (150 MHz): δ 22.8 (s, $AcCH_3$), δ 24.9 (s, $(CH_3)_2$, δ 171.55 (d, $^1J_{CN}$ 60.0 Hz, AcCO), δ 177.23 (s, CO_2H). The NMR spectra of the labelled compound are identical with those of the unlabelled acetylated α-amino isobutyric acid, with the exception of the doublets observed for the ^{15}N–H and AcCO signals.

The polycrystalline powder of [^{15}N]-acetyl-L-leucine ([^{15}N]-Ac-Leu-OH) was prepared from [^{15}N]-L-leucine

Table 1 Published amide ^{15}N chemical shift tensor principal values from solid-state NMR measurements

Sample	δ_{33}[a], ppm	δ_{22}[a], ppm	δ_{11}[a], ppm	δ_{iso}[b], ppm	$\Delta\delta$[b], ppm	η[b]	β[c], deg.	^{15}N reference[d]
n-Ac*Gly[1]	37.0 ± 2	82.8 ± 2	220.4 ± 2	113.4 ± 2	160.5	0.21	25.5° ± 1°	$^{15}NH_4Cl$ solution ≡ 27.3 ppm
(*Gly) collagen powder[1]	42.3 ± 2	67.0 ± 2	223.4 ± 2	110.9 ± 2	168.8	0.11	24.5° ± 1°	$^{15}NH_4Cl$ solution ≡ 27.3 ppm
(*Gly) collagen oriented[1]	42.3 ± 2	67.0 ± 2	223.4 ± 2	110.9 ± 2	168.8	0.11	24.5° ± 2°	$^{15}NH_4Cl$ solution ≡ 27.3 ppm
Boc-$(Gly)_2$ [^{15}N,^{2}H]Gly-Obzl[2]	55.5 ± 2	62.5 ± 2	223.4 ± 2	113.8 ± 0.5	164.4	0.03	22° ± 1°	Corrected with CH_3NO_2 ≡ 380.6 ppm
Boc-$(Gly)_2$ [^{15}N,^{2}H]Gly-OBzl[2]	36.8 ± 2	83.8 ± 2	220.8 ± 2	113.8 ± 0.5	160.5	0.21	24° ± 1°	Corrected with CH_3NO_2 ≡ 380.6 ppm
Gly*Gly[3]	48.1 ± 2	81.0 ± 2	224.2 ± 2	117.8 ± 2	159.7	0.15		Corrected with $^{15}NH_4NO_3$ ≡ 22.0 ppm
[1-^{13}C]Gly*Gly·HCl[4]	57.3 ± 3	59.8 ± 3	210.0 ± 3	109.0 ± 3	151.5	0.01	21° ± 2°[e]	$^{15}NH_4Cl$ solid ≡ 38.5
Ac[1-^{13}C]Gly*GlyNH_2[4]	40.7 ± 3	64.2 ± 3	210.6 ± 3	105.2 ± 3	158.2	0.11	20° ± 2°[e]	$^{15}NH_4Cl$ solid ≡ 38.5
Gly*Gly·HCl·H_2O (powder)[5]	59.3 ± 3	64.9 ± 3	210.3 ± 3	111.5 ± 0.2	148.2	0.03	25° ± 5°[6]	Corrected with $^{15}NH_4Cl$ solid ≡ 39.3 ppm
Gly*Gly·HCl·H_2O (crystal)[7]	58.2 ± 2	68.8 ± 2	213.8 ± 2	113.6 ± 2	150.3	0.05	21.3°[e]	Corrected with $^{15}NH_4Cl$ saturated solution ≡ 25.2 ppm
$(*Gly)_n$ β-sheet[8]	47.0 ± 2	62.7 ± 0.5	207.0 ± 2	105.5 ± 0.5	152.2	0.08		Corrected with $^{15}NH_4NO_3$ ≡ 22.0 ppm
$(*Gly)_n$ 3_1-helix[8]	51.0 ± 2	64.1 ± 0.5	216.0 ± 2	110.5 ± 0.5	158.5	0.06		Corrected with $^{15}NH_4NO_3$ ≡ 22.0 ppm
$(*Gly, Ala)_n$ α-helix[8]	46.0 ± 2	58.9 ± 0.5	214.0 ± 2	106.2 ± 0.5	161.6	0.06		Corrected with $^{15}NH_4NO_3$ ≡ 22.0 ppm
$(*Gly,Ala)_n$ β-sheet[8]	41.0 ± 2	67.3 ± 0.5	208.0 ± 2	105.5 ± 0.5	153.9	0.13		Corrected with $^{15}NH_4NO_3$ ≡ 22.0 ppm
$(*Gly,Leu)_n$ α-helix[8]	47.0 ± 2	60.7 ± 0.5	212.0 ± 2	106.5 ± 0.5	158.2	0.06		Corrected with $^{15}NH_4NO_3$ ≡ 22.0 ppm
$(*Gly,Leu)_n$ α-helix[8]	46.0 ± 2	60.9 ± 0.5	212.0 ± 2	106.4 ± 0.5	158.6	0.07		Corrected with $^{15}NH_4NO_3$ ≡ 22.0 ppm
$(*Gly,Leu)_n$ α-helix[8]	47.0 ± 2	63.0 ± 0.5	212.0 ± 2	107.3 ± 0.5	157.0	0.08		Corrected with $^{15}NH_4NO_3$ ≡ 22.0 ppm
$(*Gly,Leu)_n$ α-helix[8]	46.0 ± 2	65.0 ± 0.5	208.0 ± 2	106.4 ± 0.5	152.5	0.09		Corrected with $^{15}NH_4NO_3$ ≡ 22.0 ppm
$(*Gly,Leu)_n$ β –sheet[8]	42.0 ± 2	67.5 ± 0.5	208.0 ± 2	105.7 ± 0.5	153.3	0.12		Corrected with $^{15}NH_4NO_3$ ≡ 22.0 ppm
$(*Gly,Val)_n$ β-sheet[8]	48.0 ± 2	79.0 ± 0.5	212.0 ± 2	113.1 ± 0.5	148.5	0.15		Corrected with $^{15}NH_4NO_3$ ≡ 22.0 ppm
$(*Gly,Val)_n$ β-sheet[8]	41.0 ± 2	75.9 ± 0.5	205.0 ± 2	107.1 ± 0.5	146.6	0.17		Corrected with $^{15}NH_4NO_3$ ≡ 22.0 ppm
$(*Gly,Val)_n$ β-sheet[8]	40.0 ± 2	73.4 ± 0.5	202.0 ± 2	105.7 ± 0.5	145.3	0.17		Corrected with $^{15}NH_4NO_3$ ≡ 22.0 ppm
$(*Gly,Val)_n$ β-sheet[8]	41.0 ± 2	69.9 ± 0.5	207.0 ± 2	105.5 ± 0.5	151.6	0.14		Corrected with $^{15}NH_4NO_3$ ≡ 22.0 ppm
$(*Gly,Ile)_n$ β-sheet[8]	47.0 ± 2	69.6 ± 0.5	211.0 ± 2	109.8 ± 0.5	152.7	0.11		Corrected with $^{15}NH_4NO_3$ ≡ 22.0 ppm
$(*Gly,Lys(Z))_n$ α-helix[8]	42.0 ± 2	70.5 ± 0.5	210.0 ± 2	107.4 ± 0.5	153.8	0.14		Corrected with $^{15}NH_4NO_3$ ≡ 22.0 ppm
$(*Gly,Asp(OBzl))_n$ β-sheet[8]	41.0 ± 2	72.8 ± 0.5	210.0 ± 2	108.0 ± 0.5	153.1	0.15		Corrected with $^{15}NH_4NO_3$ ≡ 22.0 ppm
$(*Gly,Glu(OBzl))_n$ α-helix[8]	49.0 ± 2	62.5 ± 0.5	212.0 ± 2	107.8 ± 0.5	156.3	0.06		Corrected with $^{15}NH_4NO_3$ ≡ 22.0 ppm
$(*Gly,Sar)_n$[8]	40.0 ± 2	67.1 ± 0.5	206.0 ± 2	104.4 ± 0.5	152.5	0.13		Corrected with $^{15}NH_4NO_3$ ≡ 22.0 ppm
$(*Gly,Sar)_n$[8]	42.0 ± 2	69.3 ± 0.5	203.0 ± 2	104.8 ± 0.5	147.4	0.13		Corrected with $^{15}NH_4NO_3$ ≡ 22.0 ppm
$(*Gly,Sar)_n$[8]	38.0 ± 2	62.0 ± 0.5	217.0 ± 2	105.5 ± 0.5	167.0	0.11		Corrected with $^{15}NH_4NO_3$ ≡ 22.0 ppm
Val*GlyGly[9]	43.3 ± 2	78.2 ± 2	219.5 ± 2	113.7 ± 1	158.8	0.16	21° ± 1°	$^{15}NH_4Cl$ solid ≡ 39.1 ppm
Gly*GlyGly[9]	32.9 ± 2	67.5 ± 2	209.2 ± 2	103.2 ± 1	159.0	0.17		$^{15}NH_4Cl$ solid ≡ 39.1 ppm
Gly*GlyGly[9]	45.0 ± 2	65.8 ± 2	216.9 ± 2	109.2 ± 1	161.5	0.10		$^{15}NH_4Cl$ solid ≡ 39.1 ppm
Gly*GlyPhe[9]	47.2 ± 2	61.2 ± 2	216.2 ± 2	108.2 ± 1	162.0	0.06		$^{15}NH_4Cl$ solid ≡ 39.1 ppm
Gly*GlyGly[9]	41.8 ± 2	64.8 ± 2	216.6 ± 2	107.7 ± 1	163.3	0.11		$^{15}NH_4Cl$ solid ≡ 39.1 ppm

Table 1 continued

Sample	δ_{33}[a], ppm	δ_{22}[a], ppm	δ_{11}[a], ppm	δ_{iso}[b], ppm	$\Delta\delta$[b], ppm	η[b]	β[c], deg.	^{15}N reference[d]
Gly*GlyVal[9]	44.8 ± 2	72.8 ± 2	212.8 ± 2	110.1 ± 1	154.0	0.13	23.5° ± 1°	$^{15}NH_4Cl$ solid ≡ 39.1 ppm
Gly*GlyGly[9]	58.7 ± 2	68.7 ± 2	220.6 ± 2	116.0 ± 1	156.9	0.05		$^{15}NH_4Cl$ solid ≡ 39.1 ppm
Tyr*GlyGly[9]	46.6 ± 2	58.3 ± 2	209.4 ± 2	104.8 ± 1	157.0	0.06		$^{15}NH_4Cl$ solid ≡ 39.1 ppm
Gly*GlyVal[9]	55.8 ± 2	62.8 ± 2	219.8 ± 2	112.8 ± 1	160.5	0.03	20° ± 1°	$^{15}NH_4Cl$ solid ≡ 39.1 ppm
Phe*GlyGly[9]	53.2 ± 2	71.1 ± 2	223.4 ± 2	115.9 ± 1	161.3	0.08		$^{15}NH_4Cl$ solid ≡ 39.1 ppm
Pro*GlyGly[9]	51.8 ± 2	59.1 ± 2	209.2 ± 2	106.7 ± 1	153.8	0.03		$^{15}NH_4Cl$ solid ≡ 39.1 ppm
Ala*GlyGly[9]	48.5 ± 2	55.8 ± 2	210.1 ± 2	104.8 ± 1	158.0	0.03		$^{15}NH_4Cl$ solid ≡ 39.1 ppm
Ala*GlyGly[9]	39.3 ± 2	62.6 ± 2	206.6 ± 2	102.8 ± 1	155.7	0.11		$^{15}NH_4Cl$ solid ≡ 39.1 ppm
Ala*GlyGly[10] single crystal	48.0 ± 2	59.0 ± 2	207.0 ± 2	104.8 ± 0.5	153.5	0.05	23° ± 1°	$^{15}NH_4Cl$ solid ≡ 39.1 ppm
Gly*GlyVal[10] single crystal	53.0 ± 2	63.0 ± 2	218.0 ± 2	112.8 ± 0.5	160.0	0.05	20° ± 1°	$^{15}NH_4Cl$ solid ≡ 39.1 ppm
Average of 45 compounds listed above	**46.0 ± 6.3**	**67.0 ± 6.7**	**213.0 ± 6.0**	**108.7 ± 3.8**	**156.6 ± 5.6**	**0.10 ± 0.05**	**22.5°**	
(*Gly_{18}) magainin 2[11]	42.0 ± 2	73.0 ± 2	215.0 ± 2	110.0 ± 2	157.5	0.14	22° ± 2°	$^{15}NH_4Cl$ solution ≡ 27.3 ppm
(*Gly_2) gramicidin A[12]	44.0 ± 1.5	73.0 ± 1.5	219.0 ± 1.5	112.0 ± 1.5	160.5	0.13	22° ± 2°[e]	Corrected with $^{15}NH_4NO_3$ ≡ 22.0 ppm
(*Gly_{11}) PGLa[13]	35.3 ± 2	54.3 ± 2	218.3 ± 2	102.6 ± 2	173.5	0.09		Corrected with solid $^{15}NH_3Cl$ ≡ 39.3 ppm
Average of 3 compounds listed above	**40.4 ± 4.6**	**66.8 ± 10.8**	**217.4 ± 2.1**	**108.2 ± 5.0**	**163.8 ± 8.5**	**0.12 ± 0.03**	**22°**	
[1-^{13}C]Ala*Ala[14]	65.3 ± 3	78.1 ± 3	215.5 ± 3	119.6 ± 3	143.8	0.06	21° ± 2°[e]	$^{15}NH_4Cl$ solid ≡ 38.5 ppm
Ac[1-^{13}C]Gly*AlaNH_2^4	44.6 ± 3	85.1 ± 3	229.4 ± 3	119.7 ± 3	164.6	0.18	20° ± 2°[e]	$^{15}NH_4Cl$ solid ≡ 38.5 ppm
Ac[1-^{13}C]Gly*TyrNH_2^4	52.1 ± 3	77.1 ± 3	209.3 ± 3	112.8 ± 3	144.7	0.12	22° ± 2°[e]	$^{15}NH_4Cl$ solid ≡ 38.5 ppm
(*Ala)$_n$ α-helix[15]	60.3 ± 2	76.7 ± 0.5	226.3 ± 2	121.1 ± 0.5	157.8	0.07		$^{15}NH_4Cl$ solid ≡ 38.8 ppm
(*Ala)$_n$-5 β-sheet[15]	66.3 ± 2	84.0 ± 0.5	223.3 ± 2	124.5 ± 0.5	148.2	0.08		$^{15}NH_4Cl$ solid ≡ 38.8 ppm
(*Ala,Leu)$_n$ α-helix[15]	57.3 ± 2	79.2 ± 0.5	226.3 ± 2	120.9 ± 0.5	158.1	0.10		$^{15}NH_4Cl$ solid ≡ 38.8 ppm
(*Ala,Asp(OBzl))$_n$ α-helix[15]	60.3 ± 2	81.0 ± 0.5	230.3 ± 2	123.8 ± 0.5	159.7	0.09		$^{15}NH_4Cl$ solid ≡ 38.8 ppm
(*Ala,Glu(OBzl))$_n$ α-helix[15]	61.3 ± 2	79.0 ± 0.5	228.3 ± 2	122.7 ± 0.5	158.2	0.08		$^{15}NH_4Cl$ solid ≡ 38.8 ppm
(*Ala,Glu(OMe))$_n$ α-helix[15]	59.3 ± 2	80.4 ± 0.5	227.3 ± 2	122.2 ± 0.5	157.5	0.09		$^{15}NH_4Cl$ solid ≡ 38.8 ppm
(*Ala, Val)$_n$ β-sheet[15]	57.3 ± 2	84.7 ± 0.5	224.3 ± 2	122.0 ± 0.5	153.3	0.12		$^{15}NH_4Cl$ solid ≡ 38.8 ppm
(*Ala, Ile)$_n$ β-sheet[15]	62.3 ± 2	85.3 ± 0.5	222.3 ± 2	123.3 ± 0.5	148.5	0.10		$^{15}NH_4Cl$ solid ≡ 38.8 ppm
(*Asp (OBzl))$_n$-1 α_R-helix[16]	61.3 ± 2	75.1 ± 0.5	227.3 ± 2	121.2 ± 0.3	159.1	0.06		$^{15}NH_4Cl$ solid ≡ 38.8 ppm
(*Asp (OBzl))$_n$-2 α_L-helix[16]	63.3 ± 2	70.6 ± 0.5	223.3 ± 2	119.1 ± 0.3	156.4	0.03		$^{15}NH_4Cl$ solid ≡ 38.8 ppm
(*Asp (OBzl))$_n$-2 α_L-helix[16]	62.3 ± 2	69.7 ± 0.5	224.3 ± 2	118.6 ± 0.3	158.3	0.03		$^{15}NH_4Cl$ solid ≡ 38.8 ppm
(*Asp (OBzl))$_n$-2 α_L-helix[16]	63.3 ± 2	78.7 ± 0.5	225.3 ± 2	122.3 ± 0.3	154.3	0.07		$^{15}NH_4Cl$ solid ≡ 38.8 ppm
n-Ac-L-*Val-L-Leu (powder)[17]	60.2 ± 1	87.1 ± 1	230.1 ± 1	125.4 ± 0.5	156.5	0.12	20° ± 2°	$^{15}NH_4Cl$ solid ≡ 38.8 ppm
n-Ac-L-Val-L-*Leu (powder)[17]	58.7 ± 1	93.7 ± 1	232.8 ± 1	128.4 ± 0.5	156.6	0.15	18° ± 2°	Liquid NH_3 ≡ 0 ppm
n-Ac-D,L-*Val (powder) site I[17]	59.6 ± 1	80.5 ± 1	235.3 ± 1	125.1 ± 0.5	165.3	0.09	21° ± 2°	Liquid NH_3 ≡ 0 ppm
n-Ac-D,L-*Val (powder) site II[17]	57.5 ± 1	81.0 ± 1	227.0 ± 1	121.8 ± 0.5	157.8	0.10	21° ± 2°	Liquid NH_3 ≡ 0 ppm
Ala*Leu[18]	64.0 ± 1	77.0 ± 1	217.0 ± 1	119.3 ± 1	146.5	0.06		Liquid NH_3 ≡ 0 ppm

Table 1 continued

Sample	δ_{33}[a], ppm	δ_{22}[a], ppm	δ_{11}[a], ppm	δ_{iso}[b], ppm	$\Delta\delta$[b], ppm	η[b]	β[c], deg.	^{15}N reference[d]
n-Ac-D,L-*Val (powder)[19]	56.9 ± 0.5	78.3 ± 0.5	235.3 ± 1	123.5 ± 1	167.7	0.09	19° ± 2°	$(^{15}NH_4)_2SO_4$ solid ≡ 26.8 ppm
n-Ac-*Leu (powder)[20]	54.5 ± 2	94.0 ± 2	233.0 ± 2	127.3 ± 0.5	158.8	0.17		$^{15}NH_4Cl$ solid ≡ 39.1 ppm
Average of 22 compounds listed above	**59.5 ± 4.8**	**80.7 ± 6.0**	**226.0 ± 6.3**	**122.0 ± 3.3**	**156.0 ± 6.3**	**0.09 ± 0.04**	**20.25°**	
(*Leu_{14}) KL20[20]	52.5 ± 2	75.0 ± 2	227.5 ± 2	118.4 ± 0.5	163.8	0.10		$^{15}NH_4Cl$ solid ≡ 39.1 ppm
(*Phe_{16}) maganine2[11]	55.0 ± 2	80.0 ± 2	220.0 ± 2	118.3 ± 2	152.5	0.11	22° ± 3°	$^{15}NH_4Cl$ solution ≡ 27.3 ppm
(*Val_1) gramicidin A[12]	61.0 ± 1.5	85.0 ± 1.5	235.0 ± 1.5	127.0 ± 1.5	162.0	0.10	14° ± 2°[e]	Corrected with $^{15}NH_4NO_3$ ≡ 22.0 ppm
(*Ala_3) gramicidin A[12]	62.0 ± 1.5	88.0 ± 1.5	231.0 ± 1.5	127.0 ± 1.5	156.0	0.11	16° ± 2°[e]	Corrected with $^{15}NH_4NO_3$ ≡ 22.0 ppm
(D-*Leu_4) gramicidin A[12, 21]	55.0 ± 1.5	86.0 ± 1.5	221.0 ± 1.5	120.7 ± 1.5	150.5	0.14	15° ± 2°[e]	Corrected with $^{15}NH_4NO_3$ ≡ 22.0 ppm
(*Ala_5) gramicidin A[12]	60.0 ± 1.5	89.0 ± 1.5	229.0 ± 1.5	126.0 ± 1.5	154.5	0.13		Corrected with $^{15}NH_4NO_3$ ≡ 22.0 ppm
(D-*Val_6) gramicidin A[12]	59.0 ± 1.5	84.0 ± 1.5	224.0 ± 1.5	122.3 ± 1.5	152.5	0.11	15° ± 2°[e]	Corrected with $^{15}NH_4NO_3$ ≡ 22.0 ppm
(*Val_7) gramicidin A[12]	59.0 ± 1.5	82.0 ± 1.5	225.0 ± 1.5	122.0 ± 1.5	154.5	0.10		Corrected with $^{15}NH_4NO_3$ ≡ 22.0 ppm
(D-*Val_8) gramicidin A[12]	50.0 ± 1.5	77.0 ± 1.5	223.0 ± 1.5	116.7 ± 1.5	159.5	0.12		Corrected with $^{15}NH_4NO_3$ ≡ 22.0 ppm
(*Trp_9) gramicidin A[12]	59.0 ± 1.5	87.0 ± 1.5	226.0 ± 1.5	124.0 ± 1.5	153.0	0.12		Corrected with $^{15}NH_4NO_3$ ≡ 22.0 ppm
(D-*Leu_{10}) gramicidin A[12]	60.0 ± 1.5	90.0 ± 1.5	226.0 ± 1.5	125.3 ± 1.5	151.0	0.13		Corrected with $^{15}NH_4NO_3$ ≡ 22.0 ppm
(*Trp_{11}) gramicidin A[12]	58.0 ± 1.5	85.0 ± 1.5	216.0 ± 1.5	119.7 ± 1.5	144.5	0.12	14° ± 2°[e]	Corrected with $^{15}NH_4NO_3$ ≡ 22.0 ppm
(D-*Leu_{12}) gramicidin A[12]	60.0 ± 1.5	88.0 ± 1.5	218.0 ± 1.5	122.0 ± 1.5	144.0	0.13		Corrected with $^{15}NH_4NO_3$ ≡ 22.0 ppm
(*Trp_{13}) gramicidin A[12]	59.0 ± 1.5	82.0 ± 1.5	217.0 ± 1.5	119.3 ± 1.5	146.5	0.11		Corrected with $^{15}NH_4NO_3$ ≡ 22.0 ppm
(D-*Leu_{14}) gramicidin A[12]	57.0 ± 1.5	83.0 ± 1.5	220.0 ± 1.5	120.0 ± 1.5	150.0	0.12		Corrected with $^{15}NH_4NO_3$ ≡ 22.0 ppm
(*Trp_{15}) gramicidin A[12]	57.0 ± 1.5	86.0 ± 1.5	218.0 ± 1.5	120.3 ± 1.5	146.5	0.13		Corrected with $^{15}NH_4NO_3$ ≡ 22.0 ppm
(L-*Leu_{15}) orexin-B[22]	58.5 ± 3	77.5 ± 3	222.5 ± 3	119.8 ± 1.5	154.5	0.09		Corrected with NH_4Cl solid ≡ 39.3 ppm
(L-*Ala_{22}) orexin-B[22]	61.5 ± 5	84.5 ± 4	221.5 ± 5	122.3 ± 1.5	148.5	0.10		Corrected with NH_4Cl solid ≡ 39.3 ppm
(*Val_{27}) M2-TMP (res.22-46 in M2 protein in Infl. A virus)[23]	53.0 ± 2	77.0 ± 2	221.0 ± 2	117.0 ± 2	156.0	0.11		Corrected with $^{15}NH_4NO_3$ ≡ 22.0 ppm
(*Val_{28}) M2-TMP[23, 24]	51.0 ± 2	75.0 ± 2	224.0 ± 2	116.7 ± 2	161.0	0.11		Corrected with $^{15}NH_4NO_3$ ≡ 22.0 ppm
(*Ile_{32}) M2-TMP[23, 24]	57.0 ± 2	81.0 ± 2	230.0 ± 2	122.7 ± 2	161.0	0.10		Corrected with $^{15}NH_4NO_3$ ≡ 22.0 ppm
(*Ile_{33}) M2-TMP[23, 24]	53.0 ± 2	76.0 ± 2	224.0 ± 2	117.7 ± 2	159.5	0.10		Corrected with $^{15}NH_4NO_3$ ≡ 22.0 ppm
(*Ile_{35}) M2-TMP[23, 24]	54.0 ± 2	78.0 ± 2	232.0 ± 2	121.3 ± 2	166.0	0.10		Corrected with $^{15}NH_4NO_3$ ≡ 22.0 ppm
(*Ile_{39}) M2-TMP[23, 24]	52.0 ± 2	76.0 ± 2	217.0 ± 2	115.0 ± 2	153.0	0.11		Corrected with $^{15}NH_4NO_3$ ≡ 22.0 ppm
(*Leu_{40}) M2-TMP[24]	54.0 ± 2	77.0 ± 2	225.0 ± 2	118.7 ± 2	159.5	0.10		Corrected with $^{15}NH_4NO_3$ ≡ 22.0 ppm
(*Trp_{41}) M2-TMP[24]	54.0 ± 2	78.0 ± 2	227.0 ± 2	119.7 ± 2	161.0	0.11		Corrected with $^{15}NH_4NO_3$ ≡ 22.0 ppm
(*Ile_{42}) M2-TMP[23, 24]	52.0 ± 2	76.0 ± 2	220.0 ± 2	116.0 ± 2	156.0	0.11		Corrected with $^{15}NH_4NO_3$ ≡ 22.0 ppm
(*Leu_{43}) M2-TMP[24]	51.0 ± 2	78.0 ± 2	222.0 ± 2	117.0 ± 2	157.5	0.12		Corrected with $^{15}NH_4NO_3$ ≡ 22.0 ppm
(*Ala_6) alamethicin[25]	44.0 ± 2	80.0 ± 2	210.0 ± 2	111.3 ± 2	148.0	0.17		Corrected with $^{15}NH_4NO_3$ ≡ 22.0 ppm

Table 1 continued

Sample	δ_{33}[a], ppm	δ_{22}[a], ppm	δ_{11}[a], ppm	δ_{iso}[b], ppm	$\Delta\delta$[b], ppm	η[b]	β[c], deg.	^{15}N reference[d]
Average of 29 compounds listed above	**55.8 ± 4.2**	**81.4 ± 4.7**	**223.2 ± 5.4**	**120.1 ± 3.7**	**154.6 ± 5.9**	**0.11 ± 0.02**	**16°**	
Ala*ProGly single crystal[10]	38 ± 2	127 ± 2	231 ± 2	132.4 ± 0.5	98.6	0.90	20° ± 1°	$^{15}NH_4Cl$ solid ≡ 39.1 ppm

All data are referenced to liquid NH_3, $\delta \equiv 0$ ppm. Whereas data that were references with respect to liquid NH_3 are represented unmodified, corrections have been introduced as indicated in cases where δ was set to 0 for other compounds

[a] Here δ_{11}, δ_{22}, and δ_{33} are the frequency ordered ($\delta_{11} > \delta_{22} > \delta_{33}$, and the δ_{11} is the most high field) principal values of the chemical shift tensor

[b] The isotropic chemical shift $\delta_{iso} = (\delta_{11} + \delta_{22} + \delta_{33})/3$, anisotropic value $\Delta\delta = \delta_{11} - (\delta_{22} + \delta_{33})/2$ and $\eta = (\delta_{22} - \delta_{33})/\delta_{11}$

[c] The angle between the least shielded axis, δ_{11}, of the CSA tensor and the N–H bond

[d] The ^{15}N reference used in the study cited. If the reference was equivalent to liquid $NH_3 \equiv 0$ ppm, the reference was indicated and the published chemical shift tensor principal values are unchanged. Otherwise, the tensor values were adjusted accordingly

[e] These angles were calculated from given angle between δ_{11} and C–N bond assuming the angle between C–N and N–H bonds to be 120°

[1] Lee et al. (1998), [2]Hiyama et al. (1988), [3]Naito et al. (1998), [4]Oas et al. 1987), [5]Roberts et al. (1987), [6]Munowitz et al. (1982), [7]Harbison et al. (1984), [8]Shoji et al. (1998), [9]Chekmenev et al. (2004), [10]Waddell et al. (2005), [11]Lee et al. (1999), [12]Mai et al. (1993), [13]Glaser et al. (2005), [14]Hartzell et al. (1987), [15]Shoji et al. (1989), [16]Ashikawa et al. (1999), [17]Lee et al. (2001), [18]Wu et al. (1995), [19]Lee and Ramamoorthy (1998), [20]present study, [21]Teng et al. (1992), [22]Bernard et al. (2004), [23]Song et al. (2000), [24]Wang et al. (2000), [25]North et al. (1995)

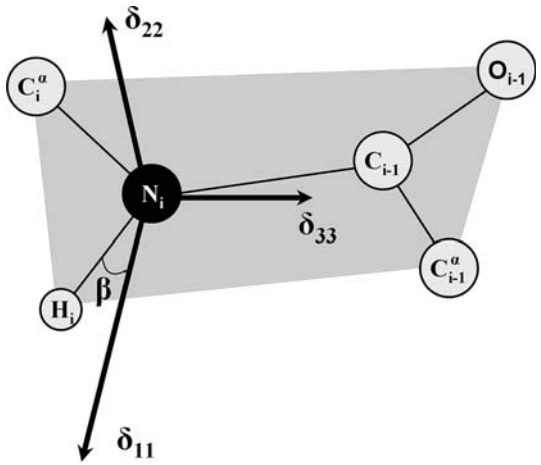

Fig. 1 The orientation of the amide ^{15}N chemical shift tensor in the peptide molecular frame. Principal values of the chemical shift tensor, δ_{11}, δ_{22}, and δ_{33}, are shown by arrows. Whereas δ_{22} is oriented perpendicular to the peptide plane, δ_{11} and δ_{33} are situated in the plane of the peptide. β is the angle between the least shielded axis, δ_{11}, of the CSA tensor and the N–H vector, it covers an angle of 15–25 degrees (see Table 1)

(Promochem, Wesel, Germany) by reaction with acetic anhydrate (Herbst and Sgemin 1943). The identity of the product was confirmed by ESI–MS.

Alamethicin labelled uniformly with ^{15}N at a level ≥92% was prepared as described previously (Yee and O'Neil 1992). The sequence of the peptide is Ac-*Aib*-Pro-*Aib*-Ala-*Aib*-*Aib*-Gln-*Aib*-Val-*Aib*-Gly-Leu-*Aib*-Pro-Val-*Aib*-*Aib*-Gln-Gln-Phol and reconstitution of this peptide into uniaxially aligned phospholipid bilayers is described in (Salnikov et al. 2009).

[U-^{15}N]-ampullosporin A, with the sequence Ac-Trp-Ala-*Aib*-*Aib*-Leu-*Aib*-Gln-*Aib*-*Aib*-*Aib*-Gln-Leu-*Aib*-Gln-Leu-OH was isolated from cultures of *Sepedonium ampullosporum* HKI-053 grown on ^{15}N enriched medium as described in (Salnikov et al. 2009). [U-^{15}N]-ampullosporin A was purified by size exclusion chromatography (Sephadex LH-20, methanol) and preparative HPLC. The products were analyzed by HPLC and their identity confirmed by mass spectrometry (Salnikov et al. 2009).

The peptide KL20 with the sequence Lys-Lys-Leu-Leu-Lys-Lys-Leu-Leu-Lys-Leu-Leu-Lys-Lys-[^{15}N]-Leu-Leu-Lys-Lys-Leu-Lys-Lys was prepared by solid-phase peptide synthesis using Fmoc chemistry and purified by reverse-phase HPLC. The ^{15}N-labelled leucine residue was incorporated at position 14 by using a ^{15}N labelled Fmoc protected L-leucine (Promochem, Wesel, Germany) as a derivative during the synthesis cycle.

Solid-state NMR spectroscopy: The proton-decoupled ^{15}N cross polarization (CP) spectra of static aligned and dry powder samples were acquired at 40.54 MHz on a Bruker Avance wide bore NMR spectrometer operating at 9.4

Tesla. An adiabatic CP pulse sequence was used with a spectral width, acquisition time, CP contact time and recycle delay of 75 kHz, 3.5 ms, 500 μs and 3 s, respectively. The ^{1}H $\pi/2$ pulse and spinal64 heteronuclear decoupling field strengths B_1 corresponded to a nutation frequency of 42 kHz. About 40,000 scans were accumulated and the spectra were zero filled to 4,092 points. An exponential line-broadening of 100 Hz was applied before Fourier transformation. Spectra were externally referenced to $^{15}NH_4Cl$ at 39.3 ppm (liquid NH_3, $\delta = 0$ ppm), however, it should be kept in mind that when screening the literature systematic deviations from this value of up to 2 ppm are found (Table 1; P. Bertani and B. Bechinger, unpublished). Samples were cooled with a stream of air at a temperature of 22°C. The two-dimensional PISEMA experiment was used to correlate the ^{15}N-^{1}H dipolar coupling with the ^{15}N chemical shift of the same nitrogen (Ramamoorthy et al. 2004) and acquired with the settings described in (Salnikov et al. 2009).

MAS spectra were obtained using a Bruker double-resonance ^{1}H/^{15}N MAS probe and a zirconium oxide rotor of 4 mm diameter on Bruker Avance wide bore spectrometers operating at ^{1}H frequencies of 400 or 500 MHz. The sample spinning rate was stabilized to the values indicated in the text within ±5 Hz.

Spectral simulations: All numerical simulations were accomplished on a 3.4-GHz Pentium(R) D workstation operating under Windows XP Professional using the SIMPSON/SIMMOL software package (Bak et al. 2000). The calculated PISEMA spectra were visualized using the GSim software, version 0.12.0. (http://www.dur.ac.uk/vadim.zorin/soft.htm). The amide ^{1}H CSA tensor of $\delta_{33} = 2.95$ ppm, $\delta_{22} = 7.95$ ppm, $\delta_{11} = 17.0$ ppm [low RF field limit (Wu et al. 1995)], and ^{15}N-^{1}H dipolar coupling of 9.9 kHz (corresponding to 1.07 Å interspin distance) were used.

In order to better represent the experimental spectra a line-broadening of 300 Hz was applied in the direct dimension and of 1 kHz in the indirect dimension. Only the ^{15}N-^{1}H dipolar couplings of the amides were taken into account by excluding the proline residues (numbers 2 and 14 in the alamethicin sequence) from the simulation.

The root mean square deviation (RMSD) was calculated from the difference between experimental and simulated spectra in the regions 30–270 ppm and 1–13.7 kHz according to: $\mathrm{RMSD} = \frac{\sqrt{\sum_{i=1}^{N}\left(I_{\mathrm{exp},i} - I_{\mathrm{sim},i}\right)^2 / N}}{noise}$, where N is the number of data points and *noise* the uncertainty of the experimental spectrum ($noise = \sqrt{\sum_{i=1}^{n} \frac{I_{\mathrm{exp},i}^2}{n}}$, where n is the number of data points of a region devoid of signal). As artifacts tend to accumulate in the spectral regions of 0 kHz dipolar splitting this area was excluded during error analysis. The simulated data were adjusted by a multiplicative factor to give the best overall agreement with the experimental data (i.e. smallest RMSD). As usual, the lower the RMSD the better the simulation fits the experimental data, with values <1 indicative of simulations that deviate from experiment only to the experimental noise level. Both tilt and pitch angles were varied to obtain the best agreement with the experimental spectrum.

Results

In order to investigate the size of the static ^{15}N tensor elements of a peptide bond formed by α-aminoisobutyric acid a powder of [^{15}N]-Ac-Aib-OH was investigated by MAS and static solid-state NMR spectroscopy (Fig. 2a, b). The resulting side-band pattern of the MAS spectrum at a spinning speed of 1 kHz and the static powder pattern line shape were simulated using the SIMPSON software (Bak et al. 2000) and are shown superimposed on the experimental spectra. The discontinuities at 68, 104 and 244 ppm are well represented by the simulation (isotropic value 140 ppm). For comparison spectra of [^{15}N]-Ac-Leu-OH were recorded and analysed in the same manner (Fig. 2c, d). The spectra were simulated using the main tensor elements 55.0, 94.5 and 233.5 ppm with an isotropic value of about 128 ppm. Notably these values are consistently reduced by about 10 ppm when compared to those obtained with [^{15}N]-Ac-Aib-OH (Table 2). Whereas the discontinuities of the powder pattern line shapes are well represented by simulation, the experimental intensity distribution of the spectra shown in Fig. 2a–d deviates from the theoretical expectation. This could be an indicator of non-homogenous cross-polarization efficiency depending on the molecular alignment relative to the magnetic field direction as has been observed previously (Frye et al. 1985; Prongidi-Fix et al. 2007).

In order to test the tensor properties of ^{15}N amides in the context of ^{15}N labelled polypeptides [U-^{15}N]-ampullosporin, [U-^{15}N]-alamethicin and [U-^{15}N]-zervamicin IIB were investigated and the data summarized in Table 2. These peptide sequences are mixtures of Aib and 'conventional' amino acids. The MAS spectrum of ampullosporin at 8 kHz spinning speed is shown in Fig. 3a and shows two isotropic peaks intensities indicating that there are two magnetically different populations of amide bonds. Deconvolution of the spectrum reveals a first peak with isotropic intensity of 115 ppm, $\Delta\nu_{1/2}$ of 13.3 ppm and an integral representing about half of the overall intensity. The second peak exhibits an isotropic maximum at 127 ppm and $\Delta\nu_{1/2}$ of 5.5 ppm. The intensity distribution reflects

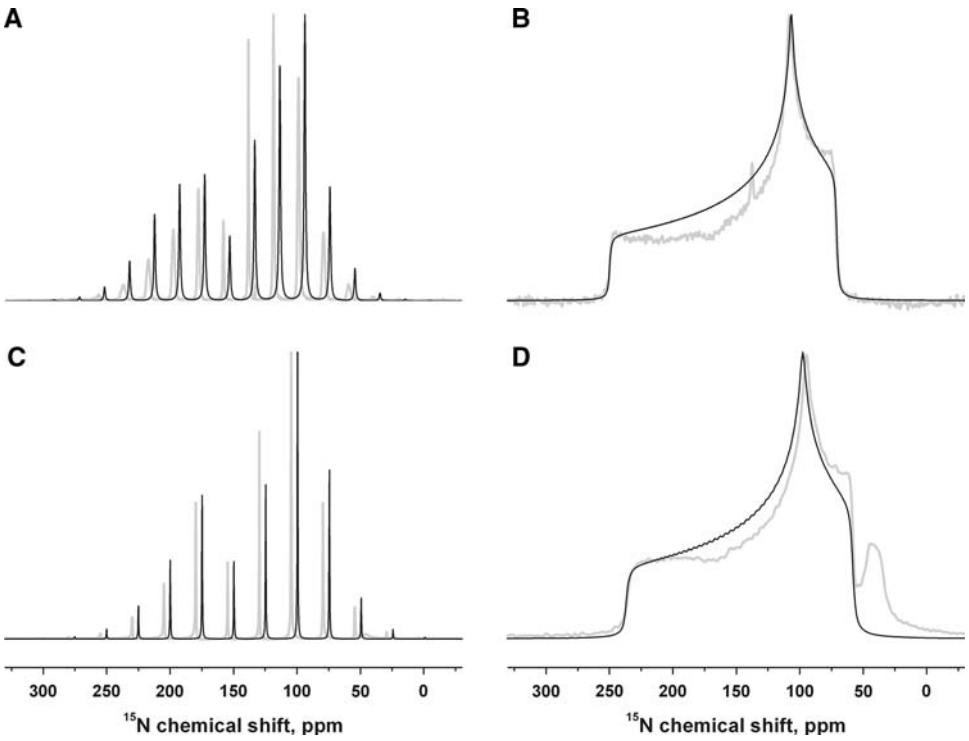

Fig. 2 Proton-decoupled ^{15}N solid-state NMR spectra (grey lines) of the dry powder of [^{15}N]-Ac-Aib-OH recorded at 11.8 Tesla, **a** 1 kHz MAS and **b** from the static sample. The simulation (smooth black line) is also shown using the main tensor elements 68, 104 and 244 ppm. Proton-decoupled ^{15}N solid-state NMR spectra of a dry powder of [^{15}N]-Ac-Leu-OH recorded at 9.4 Tesla and **c** 1 kHz MAS as well as **d** from the static sample. The additional peak at 40 ppm is probably from unreacted [^{15}N]-L-Leucine. The simulated spectra using the main tensor elements 55.0, 94.5 and 233.5 ppm is also shown. For clarity the simulations are shown shifted by 5 ppm in *panels A and C*

reasonably well the composition of ampullosporin A with seven amides formed by Aib and 8 by 'conventional' amino acids.

For the spectrum of alamethicin at 10 kHz spinning speed (Fig. 3c) very similar values are obtained with isotropic peak intensities at 116 ppm ($\Delta\nu_{1/2} = 5.9$ ppm, 48%) and at 128 ppm ($\Delta\nu_{1/2} = 7$ ppm, 52%) in agreement with the presence of 9 Aib and 11 'conventional residues', one of the latter being glycine and two being prolines (Valentine et al. 1987). The additional small peak intensities at about 105 and 140 ppm are probably due to the presence of three glutamine side chains and the Aib-1 residue (Yee and O'Neil 1992), respectively.

For comparison the spectra of a specifically ^{15}N labelled leucine within the model polypeptide KL20 are shown in Fig. 3e and f. The isotropic value of this compound, measured at 7 kHz (Fig. 3e) or 1 kHz spinning speed (Fig. 3e, insert) is 119 ppm in agreement with previous publications (Table 1).

The isotropic values measured for the *N*-acetyl model compounds are 10–15 ppm increased when compared to those observed in extended polypeptide chains and the systematic difference of >10 ppm between the amides formed by Aib and alanine, leucine or other C_α-tri-substituted residues is consistently observed. This effect is also detectable in solution where the Trp, Ala, Leu and Gln amides of alamethicin in chloroform group in the region 113–123 ppm and those of the Aibs at 126–132 ppm (Fig. 4; Table 2).

Discussion

In previous solid-state NMR studies the ^{15}N chemical shift tensors of a large number of peptides have been investigated including the amide bonds involving the nitrogens of glycine, alanine, valine, phenylalanine, leucine, isoleucine, or aspartate. The data are collected in Table 1 where special attention has been made to standardize them with reference to liquid NH_3 (Levy and Lichter 1979). Notably this reference was only introduced as a common standard after the publication of many of the data listed in Table 1 (Markley et al. 1998). As the chemical shifts of the references used in several of the papers depend on the environmental conditions such as temperature, pH or concentration (Wishart et al. 1995; P. Bertani, J. Raya, B. Bechinger, unpublished), it remains possible that some of the data exhibit systematic variations, but these are considerably smaller than the statistical errors of ±7 ppm (Table 1). Furthermore, it should be noted that temperature-dependent librational or rotational motions can cause averaging of the chemical shift anisotropy in biological samples under more physiological conditions (Hallock et al. 2000; Bechinger and Sizun 2003; Prongidi-Fix et al. 2007; Cady et al. 2007).

This detailed analysis of the published data indicates that the ^{15}N amide tensors of these peptides are described by δ_{33}, δ_{22}, δ_{11} values around 58, 81 and 225 ppm, respectively. Whereas δ_{22} is oriented perpendicular to the peptide plane, δ_{11} and δ_{33} are situated in the plane of the

Table 2 Amide ^{15}N chemical shift main tensor elements and isotropic chemical shift values of tetra-substituted (Aib, Iva) amino acids compared with the corresponding values of tri- or di-substituted proteinogenic residues

Compound	δ_{33}	δ_{22}	δ_{11}	δ_{iso} Aib/Iva	δ_{iso} Other	Method
[^{15}N]-L-Leu-OH	55.0	94.5	233.5		128	MAS, powder[a, b]
[^{15}N]-Ac-Aib-OH	68	104	244	140		MAS, powder[a]
[^{15}N-Leu^{14}]-KL20	53.0	75.5	228.0		119	MAS, powder[a, b]
[U-^{15}N]-alamethicin	64.5	85.5	232.5	128		MAS 8 kHz and powder pattern[a]
	52.5	73.5	220.5		116	
				126.0–138.7 (130.8)	114.8–120.8 (117.7)	HSQC, CD_3OH (Yee and O'Neil 1992)
					101.7 (Gly_{11})	
[U-^{15}N]-ampullosporin A	64.5	85.5	232.5	127		MAS 8 kHz and powder pattern[a]
	52.5	73.5	220.5		115	
				126.2–131.0 (128.5)	113.0–127.5 (119.3)	HSQC, CD_3OH
[U-^{15}N]-zervamicin IIB				127.7–132.1 (129.8)	111.0–125.9 (118.2)	MAS, diC10:0-PC vesicles (T. Ovchinnikova and D. Skladnev personal communication)
				124.9–132.1 (128.9)	111.0–125.9 (117.0)	NOESY, CD_3OH, (Balashova et al. 2000)
[U-^{15}N]-antiamoebin I				121.3–133.3 (125.9)	110.7–125.0 (118.0)	HSQC, CD_3OH (Shenkarev et al. 2007)
					101.1 (Gly_6)	
[^{15}N-Aib^9]-chrysospermin C				132.0		TOCSY, HMBC, DPC micelles (Anders et al. 2000)
[^{15}N-Aib^{10}]-chrysospermin C				125.5		
[^{15}N-Aib^{13}]-chrysospermin C				128.7		

For solution NMR spectra the averages are given in brackets

[a] The isotropic values were extracted from the MAS solid-state (Figs. 2, 3) and solution HSQC NMR spectra (Fig. 4), while the tensor values were determined from the fits of the powder pattern line shapes (Figs. 2, 3)

[b] Also included in Table 1

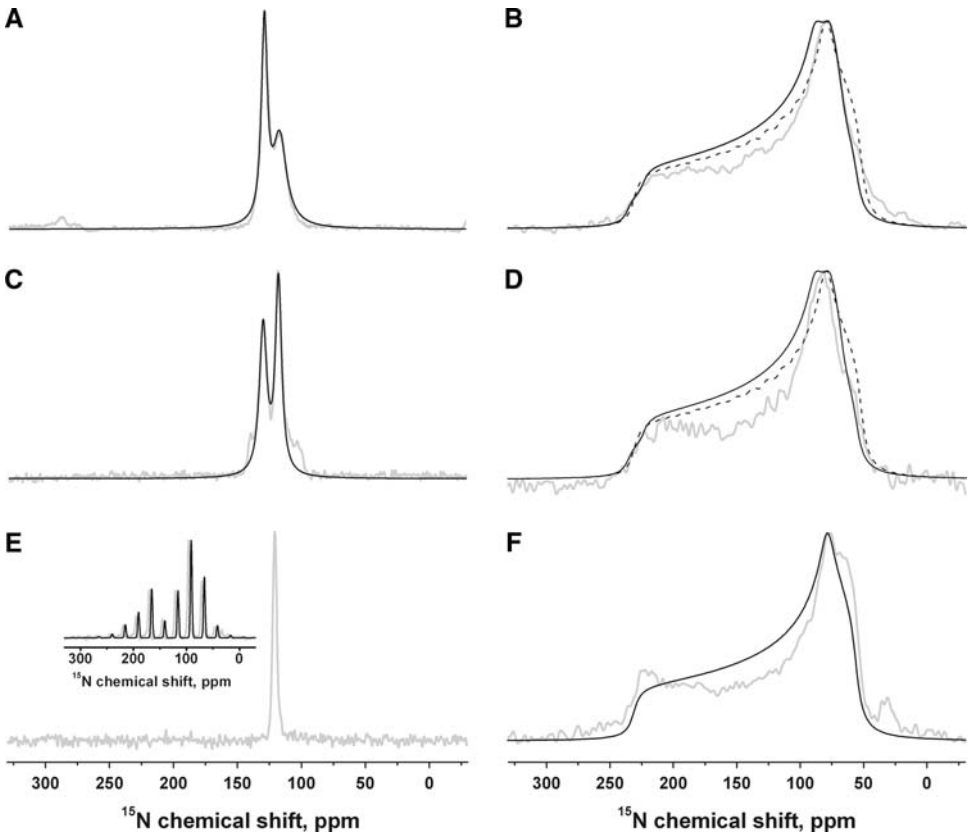

Fig. 3 Proton-decoupled ^{15}N solid-state NMR spectra of non-oriented ampullosporin A (**a**, **b**) and of alamethicin (**c**, **d**), both uniformly labelled with ^{15}N, and of KL20 labelled at a single site with ^{15}N-Leu (**e**–**f**). The MAS spectra were recorded at spinning speeds of 8 kHz (**a**), 10 kHz (**c**), 7 kHz (**e**) and 1 kHz (*insert* in panel **e**). Experimental ^{15}N NMR solid-state NMR spectra of the non-oriented static peptide powders are shown by *grey lines* in **b**, **d** and **f**. Panels **b** and **d** also show spectral simulations using the main tensor elements (64.5, 85.5 and 232.5 ppm) for Aib and (52.5, 73.5 and 220.5 ppm) for all other residues (*dark solid lines*), or by using a unique tensor for all residues (49.0, 76.5 and 228.0 ppm; *dashed lines*). The chemical shift tensor main elements used for the simulation of the spectrum shown in **f** and in the insert in panel **e** are 52.5, 75.0 and 227.5 ppm. For clarity the simulations are shown shifted by 5 ppm in the insert in panel **e**

peptide bond where δ_{11} and the N–H vector cover an angle of 15–25 degrees (cf. Table 1; Fig. 1). The glycine values are about 12 ppm reduced when compared to those of the other 'conventional' amino acids (Ala, Leu, Val, etc.) when at the same time the chemical shift anisotropy is maintained. The experimental data and quantum chemical calculations indicate that the main tensor elements within the molecular frame are subject to relatively small variations in their alignment [references cited in (Brender et al. 2001) and Table 1].

When investigated in more detail the secondary structure of a peptide has a pronounced influence on the tensor and in particular the δ_{22} values (Poon et al. 2004; Shoji et al. 1990, 1998). Therefore it is important to note that the peptides investigated in this work all show a high propensity for helix conformations in the crystal structure, in organic solvents or in membrane environments (Yee et al. 1995; Kronen et al. 2003; Salnikov et al. 2009; Vogt et al. 2000).

Notably, the comparison of the ^{15}N-tensor values of the powder patterns of the *N*-acetyl amino acids and the polypeptides investigated here (Figs. 2, 3; Table 2) indicates that the former are characterized by discontinuities that are up to 20 ppm increased when compared to the latter. It is possible that intermolecular interactions such as H-bonding or different dihedral angles are the reason for the shift observed for the smaller molecules as has been observed with some dipeptides (Poon et al. 2004).

When [^{15}N]-Ac-Aib-OH and [^{15}N]-Ac-Leu-OH are compared to each other the static chemical shift tensor elements and the isotropic ^{15}N chemical shift values differ by about 10–15 ppm. This is in agreement with the occurrence of two clearly different isotropic chemical shift positions in the MAS solid-state NMR spectra (Fig. 3a, c) or in the HSQC spectra of peptaibols in organic solvents (Fig. 4; Table 2). Furthermore, the powder pattern line shapes obtained from the peptaibols are best simulated when taking into account two different ^{15}N chemical shift

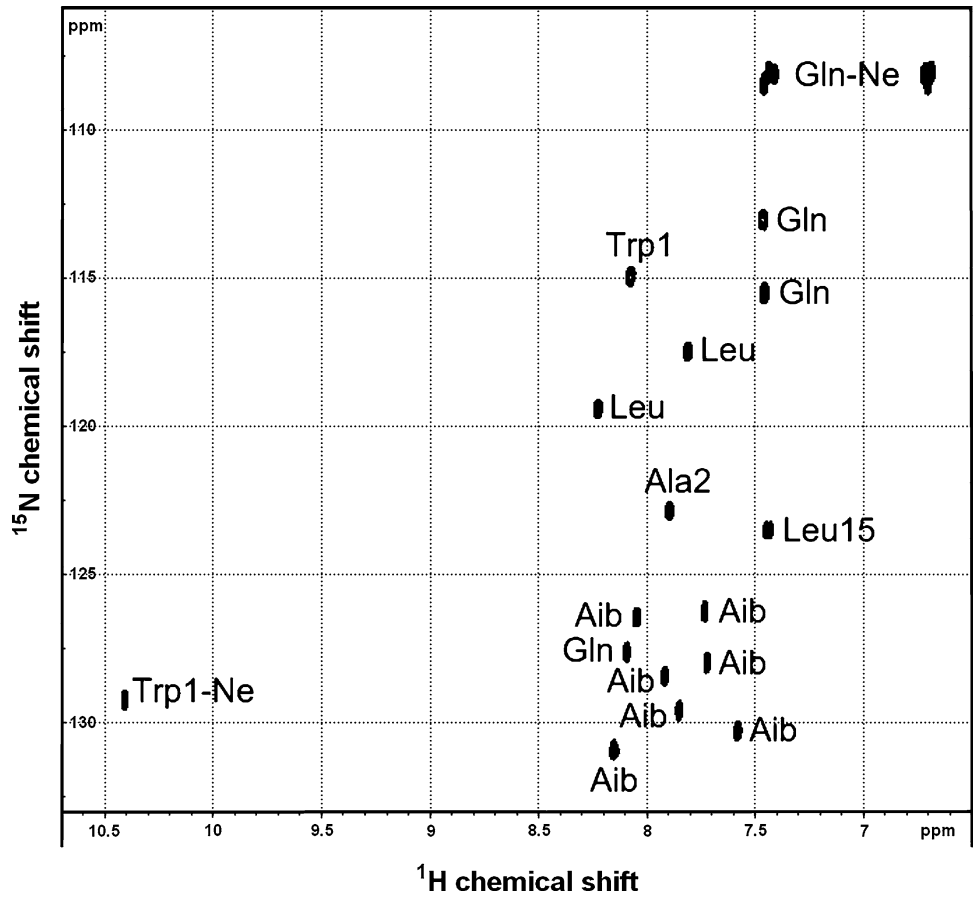

Fig. 4 HSQC spectrum of uniformly ^{15}N labelled ampullosporin A in CD_3OH with partial assignments

tensors, where the one describing the Aib residues is in the range 64.5/85.5/232.5 ppm (Fig. 3b, d; Table 2).

Glycine, alanine (and other proteinogenic amino acids) and α-aminoisobutyric acid (as well as isovaline) residues might be characterized as bi-, tri- and tetra-substituted, respectively, by taking into account the number of C–C and C–N bonds linked to the C_α atoms. In parallel the averages of the isotropic ^{15}N chemical shift increases from 109 ppm, via 121 ppm to about 130 ppm (Tables 1, 2; Eldon et al. 2007) in agreement with quantum chemical calculations which indicated that glycine (and proline) should be considered separately in structural studies (Poon et al. 2004). As the overall line shape of the spectra, as described by the anisotropy ($\Delta\delta$) and the asymmetry parameters (η; cf Table 1, footnote b for definition) are unchanged the difference in isotropic chemical shift is also reflected in δ_{33}, δ_{22} and δ_{11}, which all follow an about 10 ppm stepwise increase when going from di- to tri- and to tetra-substituted residues (Table 2; Vosegaard et al. 2008).

The PISEMA spectrum of alamethicin reconstituted into oriented POPC lipid bilayers correlates the ^{15}N chemical shift and the ^{1}H–^{15}N dipolar coupling of the individual sites and thereby provides additional resolution and structural information. Figure 5a–f shows the simulations of PISEMA spectra that arise from different polypeptide conformations superimposed onto the experimental spectrum (light grey). The upper row of the Figure shows the simulations when a unique tensor is used for all sites, which was found from the quantitative analysis of the powder pattern spectra (dashed lines in Fig. 3b, d). The spectra of the row below were calculated using different tensors for Aib and 'conventional' amino acid residues. The simulations shown in Fig. 5a–c were carried out using the coordinates of the three crystallographically independent alamethicin molecules in the unit cell of the alamethicin crystal (Fox and Richard 1982). The simulations shown in panels D-E are for ideal α-, 3_{10}- or mixed α-/3_{10}-helix conformations, respectively. Some of these spectra are characterized by regular features such as a 'helical wheel' (Fig. 5d) or the overlap of signal intensities in three well defined spectral regions as expected for a 3_{10}-helix (Fig. 5e). When the two data sets are compared to each other it becomes evident that the simulated spectra are clearly different and many of the regular features observed when using a unique tensor are less apparent in the dual tensor approach although the

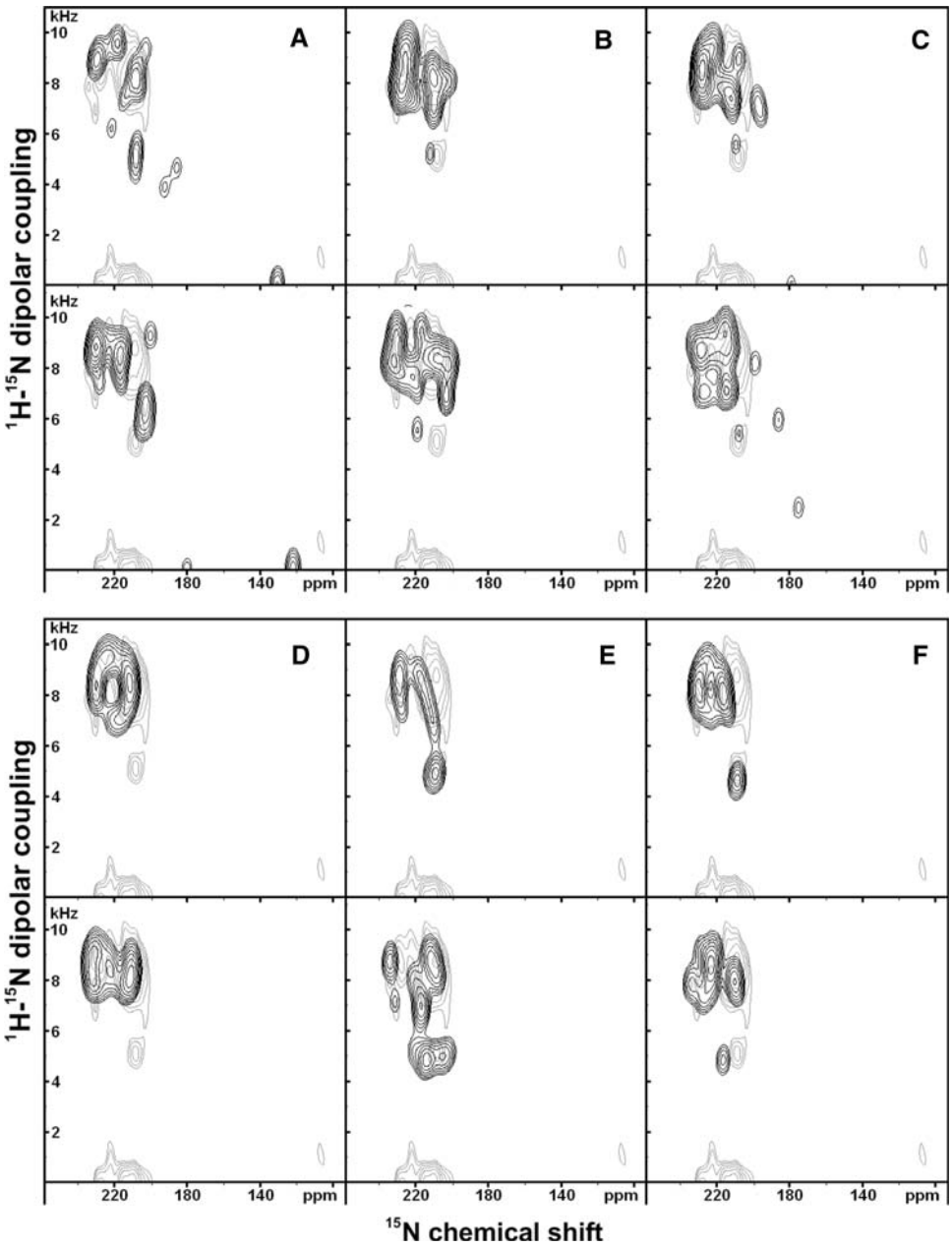

Fig. 5 PISEMA spectra of [U-^{15}N]-alamethicin in POPC (peptide-to-lipid 1:100) using a unique ^{15}N chemical shift tensor (*top row*) or different chemical shift tensors for Aib and all other residues (*bottom row*). Simulations of the NMR spectra resulting from different secondary structures (*black*) are superimposed on the experimental spectrum (*light grey*). **a** alamethicin structure (pdb: 1AMT), unit A. **b** alamethicin structure, unit B. **c**: alamethicin structure, unit C. **d**: model α-helical ($\varphi = -65°$, $\psi = -45°$) peptide. **e** model 3_{10}-helical ($\varphi = -50°$, $\psi = -31°$) peptide. **f** mixed α-/3_{10}-helical model peptide (the first 10 residues folded in α-helix and the last 10 residues in 3_{10}-helix). Tilt angles and RMSD values are collected in Table 3

secondary structure of the molecule has not been altered. Table 3 summarizes the results of these simulations where in each case the secondary structures were aligned in such a manner to best fit the experimental spectrum. Whereas the fits are of similar quality (in some instances the use of the unique tensor even seems to give a slightly better result), the spectra shown in Figs. 3 and 4 clearly indicate that the tensors of Aib and tri-substituted amino acids are shifted when compared to each other, therefore, the dual set of tensors should be used. Whereas the quality of fit criterium cannot be used to select one set of tensors over the other the optimal tilt angle that results from the selection of the unique or dual tensor varies by up to 6 degrees (Table 3). Notably, in view of the considerable variations of the ^{15}N chemical shift tensors (Table 1) similar considerations also apply to the structural analysis of membrane-associated polypeptides composed solely of 'conventional' residues with regard to the resulting accuracies of the structures and tilt angles. However, the structural resolution can be improved by determining the tensor for every residue individually, by MD simulations, or by supplementary data, such as independent secondary structure information, from which the tensor variation could be reduced.

Table 3 Helical tilt angle information and RMSD values derived from the simulations of the experimental PISEMA data of alamethicin in oriented POPC bilayers using either a unique amide ^{15}N CSA tensor for all residues (49.0, 76.5 and 228.0 ppm), or different amide ^{15}N CSA tensors for Aib (64.5, 85.5 and 232.5 ppm) and for all other residues (52.5, 73.5 and 220.5 ppm). These tensor elements fit best the ^{15}N NMR powder spectra of alamethicin (Fig. 3d). The corresponding experimental spectrum and the simulations are shown in Fig. 5

Structural model	Unique CSA tensor		Dual CSA tensor	
	Tilt angle, degree	RMSD	Tilt angle, degree	RMSD
XRD structure, unit A	11.6[a]	1.25	6[a]	1.34
XRD structure, unit B	7.3[a]	1.31	8[a]	1.29
XRD structure, unit C	3.2[b]	1.36	8.4[b]	1.30
α-Helix	9.9	1.30	6.3	1.32
3_{10}-Helix	14.2	1.30	14	1.29
Mixed α/3_{10}-helix	9.5	1.36	8.7	1.32

[a] Residues number 1–11 (N-terminal part)

[b] 8 N-terminal residues

Acknowledgments We acknowledge Herdis Friedrich, Siegmund Reissmann, Christian Hertweck, Xing Li and Joe D. J. O'Neil for the kind gifts of labelled ampullosporin and alamethicin, respectively as well as Lionel Allouche and Roland Graff for acquiring the HSQC spectrum. This work was supported by the Dutch-Russian Research Cooperation Program (Netherlands Organization of Scientific Research in collaboration with the Russian Foundation of Basic Research, NWO 047.017.034), the Agence Nationale pour la Recherche, the RMN Grand-Est Network of the French Ministry of Research and Vaincre la Mucoviscidose (TG0602). E.S.S. greatly thanks the French government fellowship program (BGF) for financial support. The Institute of Supramolecular Chemistry of the University of Strasbourg (ISIS) is acknowledged for hosting the Bechinger laboratory.

References

Aisenbrey C, Bechinger B (2004) Investigations of peptide rotational diffusion in aligned membranes by ^{2}H and ^{15}N solid-state NMR spectroscopy. J Am Chem Soc 126:16676–16683

Aisenbrey C, Sizun C, Koch J, Herget M, Abele U, Bechinger B, Tampe R (2006) Structure and dynamics of membrane-associated ICP47, a viral inhibitor of the MHC I antigen-processing machinery. J Biol Chem 281:30365–30372

Anders R, Ohlenschlager O, Soskic V, Wenschuh H, Heise B, Brown LR (2000) The NMR solution structure of the ion channel peptaibol chrysospermin C bound to dodecylphosphocholine micelles. Eur J Biochem 267:1784–1794

Ashikawa M, Shoji A, Ozaki T, Ando I (1999) Nitrogen-15 chemical shift tensors and conformation of poly(*β*-benzyl L-aspartate) in the solid state by NMR. Macromolecules 22:2288–2292

Bak M, Rasmussen JT, Nielsen NC (2000) SIMPSON: a general simulation program for solid-state NMR spectroscopy. J Magn Res 147:296–330

Balashova A, Shenkarev O, Tagaev A, Ovchinnikova V, Raap J, Arseniev S (2000) NMR structure of the channel-former zervamicin IIB in isotropic solvents. FEBS Lett 466:333–336

Bax A, Grishaev A (2005) Weak alignment NMR: a hawk-eyed view of biomolecular structure. Curr Opin Struct Biol 15:563–570

Bechinger B (1997) Structure and functions of channel-forming polypeptides: magainins, cecropins, melittin and alamethicin. J Membrane Biol 156:197–211

Bechinger B (2009) Solid-state NMR approaches to measure topological equilibria and dynamics of membrane polypeptides. Biochim Biophys Acta (in press)

Bechinger B, Sizun C (2003) Alignment and structural analysis of membrane polypeptides by ^{15}N and ^{31}P solid-state NMR spectroscopy. Concepts Magn Reson 18A:130–145

Bechinger B, Zasloff M, Opella SJ (1993) Structure and orientation of the antibiotic peptide magainin in membranes by solid-state NMR spectroscopy. Protein Sci 2:2077–2084

Bernard GM, Miskolzie M, Kotovich G, Wasylishen RE (2004) A solid-state NMR investigation of orexin-B. Can J Chem 82:1554–1563

Brender JR, Taylor DM, Ramamoorthy A (2001) Orientation of amide-nitrogen-15 chemical shift tensors in peptides: a quantum chemical study. J Am Chem Soc 123:914–922

Cady SD, Goodman C, Tatko CD, DeGrado WF, Hong M (2007) Determining the orientation of uniaxially rotating membrane proteins using unoriented samples: a ^{2}H, ^{13}C, and ^{15}N solid-state NMR investigation of the dynamics and orientation of a transmembrane helical bundle. J Am Chem Soc 129:5719–5729

Chekmenev EY, Zhang Q, Waddell KW, Mashuta MS, Wittebort RJ (2004) ^{15}N chemical shielding in glycyl tripeptides: measurement by solid-state NMR and correlation with X-ray structure. J Am Chem Soc 126:379–384

Cross TA (1997) Solid-state nuclear magnetic resonance characterization of gramicidin channel structure. Methods Enzymol 289:672–696

Dürr UHN, Yamamoto K, Im SC, Waskell L, Ramamoorthy A (2007) Solid-state NMR reveals structural and dynamical properties of a membrane-anchored electron-carrier protein, cytochrome b(5). J Am Chem Soc 129:6670–6671

Eldon LU, Akutsu H, Doreleijers JF, Harano Y, Ionnidis YE, Lin J, Livny M, Mading S, Maziuk D, Miller Z, Nakatani E, Schulte CF, Tolmie DE, Wenger RK, Hongyang Y, Markley JL (2007) BioMagResBank. Nucleic Acids Res 36:D402–D408

Frye J, Albert AD, Selinsky BS, Yeagle PL (1985) Cross polarization P-31 nuclear magnetic resonance of phospholipids. Biophys J 48:547–552

Glaser RW, Sachse C, Durr UHN, Wadhwani P, Afonin S, Strandberg E, Ulrich AS (2005) Concentration-dependent realignment of the antimicrobial peptide PGLa in lipid membranes observed by solid-state ^{19}F-NMR. Biophys J 88:3392–3397

Hallock KJ, Lee DK, Ramamoorthy A (2000) The effects of librations on the ^{13}C chemical shift and ^{2}H electric field gradient tensors in beta-calcium formate. J Chem Phys 113:11187–11193

Harbison G, Jelinski L, Stark R, Torchia D, Herzfeld G, Griffin R (1984) ^{15}N chemical shift and ^{15}N–^{13}C dipolar tensors for the peptide bond in [1–^{13}C]glycyl[^{15}N]glycine hydrochloride monohydrate. J Magn Res 60:79–82

Hartzell CJ, Whitfield M, Oas TG, Drobny GP (1987) Determination of the ^{15}N and ^{13}C chemical shift tensors of L-[^{13}C]alanyl-L-[^{15}N]alanine from the dipole-coupled powder patterns. J Am Chem Soc 109:5966–5969

Herbst RM, Sgemin D (1943) Acetylglycine. Org Synth 2:11–12

Hiyama Y, Niu CH, Silverton JV, Bavoso A, Torchia D (1988) Determination of ^{15}N chemical shift tensor via ^{15}N–^{2}H dipolar coupling in Boc-glycylglycyl[^{15}N]glycine benzyl ester. J Am Chem Soc 110:2378–2383

Kronen M, Gorls H, Nguyen HH, Reissmann S, Bohl M, Suhnel J, Grafe U (2003) Crystal structure and conformational analysis of ampullosporin A. J Pept Sci 9:729–744

Lee D, Ramamoorthy A (1998) A simple one-dimensional solid-state NMR method to characterize the nuclear spin interaction tensors associated with the peptide bond. J Magn Res 133:204–206

Lee D, Wittebort RJ, Ramamoorthy A (1998) Characterization of ^{15}N chemical shift and ^{1}H–^{15}N dipolar coupling interactions in a peptide bond of uniaxially oriented and polycrystalline samples by one-dimensional dipolar chemical shift solid-state NMR spectroscopy. J Am Chem Soc 120:8868–8874

Lee D, Santos JS, Ramamoorthy A (1999) Nitrogen-15 chemical shift anisotropy and ^{1}H–^{15}N dipolar coupling tensors associated with the phenylalanine residue in the solid state. Chem Phys Lett 309:209–214

Lee D, Wei Y, Ramamoorthy A (2001) A two-dimensional magic-angle decoupling and magic-angle turning solid-state NMR method: An application to study chemical shift tensors from peptides that are nonselectively labeled with ^{15}N isotope. J Phys Chem B 105:4752–4762

Levy GC, Lichter LU (1979) ^{15}N NMR spectroscopy. Wiley, NY

Lipsitz RS, Tjandra N (2004) Residual dipolar couplings in NMR structure analysis. Annu Rev Biophys Biomol Struct 33:387–413

Mai W, Hu W, Wang C, Cross TA (1993) Orientational constraints as three-dimensional structural constraints from chemical shift anisotropy: The polypeptide backbone of gramicidin A in a lipid bilayer. Protein Sci 2:532–542

Markley JL, Bax A, Arata Y, Hilbers CW, Kaptein R, Sykes BD, Wright PE, Wüthrich K (1998) Recommendations for the presentation of NMR structures of proteins and nucleic acids. Pure & Appl Chem 70:117–142

Mehring M (1983) Principles of high resolution NMR in solids. Springer, Berlin

Munowitz MG, Aue WP, Griffin RG (1982) Two-dimensional separation of dipolar and scaled isotropic chemical shift interactions in magic angle NMR spectra. J Chem Phys 77:1686–1689

Naito A, Fukutani A, Uitdehaag M, Tuzi S, Saito H (1998) Backbone dynamics of polycrystalline peptides studied by measurements of ^{15}N NMR lineshapes and ^{13}C transverse relaxation times. J Mol Struct 441:231–241

North CL, Barranger-Mathys M, Cafiso DS (1995) Membrane orientation of the N-terminal segment of alamethicin determined by solid-state ^{15}N NMR. Biophys J 69:2392–2397

Oas TG, Hartzell CJ, Dahlquist FW, Drobny GP (1987) The amide ^{15}N chemical shift tensors of four peptides determined from ^{13}C dipole-coupled chemical shift powder patterns. J Am Chem Soc 109:5962–5966

Ogrel A, Shvets VI, Kaptein B, Broxterman QB, Raap J (2000) Synthesis of ^{15}N-labelled D-isovaline and α-aminoisobutyric acid. Eur J Org Chem 2000:857–859

Opella SJ, Zeri AC, Park SH (2008) Structure, dynamics, and assembly of filamentous bacteriophages by nuclear magnetic resonance spectroscopy. Annu Rev Phys Chem 59:635–657

Poon A, Birn J, Ramamoorthy A (2004) How does an amide-N-15 chemical shift tensor vary in peptides? J Phys Chem B 108:16577–16585

Prestegard JH, Bougault CM, Kishore AI (2004) Residual dipolar couplings in structure determination of biomolecules. Chem Rev 104:3519–3540

Prongidi-Fix L, Bertani P, Bechinger B (2007) The membrane alignment of helical peptides from non-oriented ^{15}N chemical shift solid-state NMR spectroscopy. J Am Chem Soc 129:8430–8431

Prosser RS, Evanics F, Kitevski JL, Al-Abdul-Wahid MS (2006) Current applications of bicelles in NMR studies of membrane-associated amphiphiles and proteins. Biochemistry 45:8453–8465

Ramamoorthy A, Wei Y, Lee D (2004) PISEMA solid-state NMR spectroscopy. Annual Reports NMR Spectrosc 52:1–52

Roberts JE, Harbison G, Munowitz MG, Herzfeld G, Griffin RG (1987) Measurement of heteronuclear bond distances in polycrystalline solids by solid-state NMR techniques. J Am Chem Soc 109:4163–4169

Salnikov ES, Friedrich H, Li X, Bertani P, Reissmann S, Hertweck C, O'Neil JD, Raap J, Bechinger B (2009) Structure and alignment of the membrane-associated peptaibols ampullosporin A and alamethicin by oriented ^{15}N and ^{31}P solid-state NMR spectroscopy. Biophys J 96:86–100

Sansom MS (1993) Alamethicin and related peptaibols–model ion channels. Eur Biophys J 22:105–124

Shenkarev ZO, Nadezhdin KD, Bocharov EV, Kudelina IA, Skladnev DA, Tagaev AA, Yakimenko ZA, Ovchinnikova TV, Arseniev AS (2007) Antiamoebin I in methanol solution: rapid exchange between right-handed and left-handed 3(10)-helical conformations. Chem Biodivers 4:1219–1242

Shoji A, Ozaki T, Fujito T, Deguchi K, Ando S, Ando I (1989) ^{15}N NMR chemical shift tensors and conformation of some ^{15}N-labeled polypeptides in the solid state. Macromolecules 22:2863

Shoji A, Ozaki T, Fujito T, Deguchi K, Ando S, Ando I (1990) ^{15}N chemical shift tensors and conformation of solid polypeptides containing ^{15}N-labeled L-alanine residue by ^{15}N NMR. 2. Secondary structure reflected in σ_{22}. J Am Chem Soc 112:4693–4697

Shoji A, Ozaki T, Fujito T, Deguchi K, Ando I, Magoshi J (1998) ^{15}N chemical shift tensors and conformation of solid polypeptides containing ^{15}N-labeled glycine residue by ^{15}N NMR. J Mol Struct 441:251–266

Song Z, Kovacs FA, Wang J, Denny JK, Shekar SC, Quine JR, Cross TA (2000) Transmembrane domain of M2 protein from Influenza A virus studied by solid-state ^{15}N polarization inversion spin exchange at magic angle NMR. Biophys J 79:767–775

Teng Q, Iqbal M, Cross TA (1992) Determination of the ^{13}C chemical shift and ^{14}N electric field gradient tensor orientations with respect to the molecular frame in a polypeptide. J Am Chem Soc 114:5312–5321

Tolman JR, Ruan K (2006) NMR residual dipolar couplings as probes of biomolecular dynamics. Chem Rev 106:1720–1736

Valentine KG, Rockwell AL, Gierasch LM, Opella SJ (1987) ^{15}N chemical-shift tensor of the imide nitrogen in the alanyl-prolyl peptide bond. J Magn Res 73:519–523

Vogt TCB, Ducarme P, Schinzel S, Brasseur R, Bechinger B (2000) The topology of lysine-containing amphipathic peptides in bilayers by CD, solid-state NMR and molecular modeling. Biophys J 79:2644–2656

Vosegaard T, Bertelsen K, Pedersen JM, Thogersen L, Schiott B, Tajkhorshid E, Skrydstrup T, Nielsen NC (2008) Resolution

enhancement in solid-state NMR of oriented membrane proteins by anisotropic differential linebroadening. J Am Chem Soc 130:5028–5029

Waddell KW, Chekmenev EY, Wittebort RJ (2005) Single-crystal studies of peptide prolyl and glycyl ^{15}N shielding tensors. J Am Chem Soc 127:9030–9035

Wang J, Denny JK, Tian C, Kovacs F, Song Z, Fu R, Quine JR, Cross TA, Kim S, Mo Y, Nishimura K, Gan Z (2000) Imaging membrane protein helical wheels. J Magn Res 144:162–167

Wishart DS, Bigam CG, Yao J, Abildgaard F, Dyson HJ, Oldfield E, Markley JL, Sykes BD (1995) ^{1}H, ^{13}C and ^{15}N chemical shift referencing in biomolecular NMR. J Biomol NMR 6:135–140

Wu CH, Ramamoorthy A, Gierasch LM, Opella SJ (1995) Simultaneous characterization of the amide ^{1}H chemical shift, ^{1}H–^{15}N dipolar, and ^{15}N chemical shift interaction tensors in a peptide bond by three-dimensional solid-state NMR spectroscopy. J Am Chem Soc 117:6148–6149

Yee AA, O'Neil JD (1992) Uniform ^{15}N labeling of a fungal peptide: the structure and dynamics of an alamethicin by ^{15}N and ^{1}H NMR spectroscopy. Biochemistry 31:3135–3143

Yee AA, Babiuk R, O'Neil JDJ (1995) The conformation of an alamethicin in methanol by multinuclear NMR spectroscopy and distance geometry simulated annealing. Biopolymers 36: 781–792